ACS OMEGA

http://pubs.acs.org/journal/acsodf

Article

Investigation on the Redox Properties of a Novel Cu-Based Pr-Modified Oxygen Carrier for Chemical Looping Combustion

Muhammad Qasim, Muhammad Ayoub,* Aqsha Aqsha, Nur Adibah Ghazali, Sami Ullah, Yoshito Ando, and Sarah Farrukh

Cite This: *ACS Omega* 2022, 7, 40789−40798

Read Online

ACCESS | Metrics & More | Article Recommendations

ABSTRACT: CO_2 levels in the atmosphere are growing as a result of the burning of fossil fuels to meet energy demands. The introduction of chemical looping combustion (CLC) as an alternative to traditional combustion by transporting oxygen emphasizes the need to develop greener and more economical energy systems. Metal oxide, also defined as an oxygen carrier (OC), transports oxygen from the air to the fuel. Several attempts are being made to develop an OC with a reasonable material cost for superior fuel conversion and high oxygen transport capacity (OTC). This study aims to synthesize a potential OC using the wet impregnation method for the CLC process. Thermogravimetric analysis (TGA) was used to determine the cyclic redox properties using 5% CH_4/N_2 and air as reducing and oxidizing gases, respectively. The 10CuPA-based OC retained a high OTC of about 0.0267 mg O_2/mg of OC for 10 cycles that was higher than 10CuA-based OC. Furthermore, the oxygen transfer rate for 10CuPA-based OC was relatively higher compared to 10CuA-based OC over 10 cycles. In comparison to 10CuA-based OC, the 10CuPA-based OC presented a steady X-ray diffraction (XRD) pattern after 10 redox cycles, implying that the phase was stably restored due to praseodymium-modified γ alumina support.

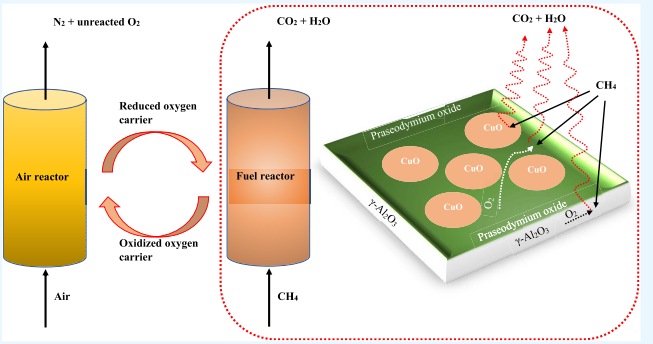

1. INTRODUCTION

The most extensively consumed sources of energy for electricity production are fossil fuels. Furthermore, fossil fuels contributed to more than 85% of the total energy demand. Power plants that combust fossil fuels release an excess amount of CO_2, which is the primary source of greenhouse gases caused by humans. Consequently, in the past couple of years, countries all over the world have been attempting to minimize CO_2 release after the combustion of fossil fuels.[1−3] Chemical looping combustion (CLC) promises a realistic alternative for CO_2 capture with relatively minimal cost.[4,5] The dominant element of the CLC process is a metal oxide, also known as oxygen carrier (OC), that transfer oxygen from an air reactor to a fuel reactor while avoiding air and fuel interaction. The reduced OC is recycled to the air reactor after fuel combustion and oxidized with O_2 (air) for upcoming cycles. During this cyclic circulation of OC, the outlet gases from the air reactor consist of N_2 and unreacted O_2. On the other hand, the outlet gases from the fuel reactor comprise CO_2 and H_2O (vapors). After condensing vapors, the produced CO_2 can easily be captured without any additional equipment cost for the separation. The essential characteristics of OCs are that OCs should have high oxygen transport capacity (OTC) and mechanical and thermal stabilities.[6−8]

A number of materials have been studied as OCs for the CLC process in recent years.[9] For this purpose, transition metal oxides, such as CuO,[10,11] Fe_2O_3,[12,13] NiO,[14,15] Mn_3O_4,[16,17] and Co_2O_3,[18] have been investigated as OCs. Across all monometallic oxide-based OCs, NiO and CuO exhibited the highest OTCs, 21 and 20 wt %, respectively. The investigation of the CLC process for the combustion of natural gas was carried out in 10−140 kWth plants using Ni- and Cu-based OCs.[19−22] In the process of methane reforming, NiO is considered an excellent material, but for the CLC of methane, NiO exhibited poor performance due to carbon deposition.[23] However, the reactivity of Cu-based OCs in the oxidation and reduction cycles was high.[24] Furthermore, Cu-based OCs can release O_2 (gas-phase oxygen) during the combustion of solid fuels at a temperature greater than 700 °C.[10] In addition, Cu-based OCs are environmentally friendly and less expensive as compared to Ni and Co. However, the low Tammann

Received: May 13, 2022
Accepted: August 26, 2022
Published: November 1, 2022

temperature (the Tammann temperature determines the commencement of bulk material sintering) of the CuO/Cu (or CuO/Cu_2O) redox pair is the main obstacle concerned with using CuO-based OCs, despite their promising properties. Therefore, pure CuO-based OCs result in the sintering and agglomeration of OC particles at high temperatures. In addition, during the circulation of OC particles in fluidized bed reactors, the structure of OCs significantly changed by agglomeration that ensures the deactivation of a fluidized bed. Therefore, the Cu-based OCs using different support materials such as γ-Al_2O_3,[25,26] TiO_2,[27] CeO_2,[28] and ZO_2[29] have been investigated to prevent agglomeration. Among these support materials, γ-Al_2O_3 was the most studied material due to its low attrition rate, large surface area, and excellent stability.[30,31] However, previous research works examined that the particles of Cu-based OCs undergo agglomeration at high temperatures besides using these supports. For example, the activity loss was observed for 60 wt % Cu−CeO_2 due to agglomeration during few redox cycles.[32] The interaction between Cu contents and γ-Al_2O_3 support at high temperatures resulted in a highly stable spinel ($CuAl_2O_4$) compound.[33,34] This spinel compound causes loss of Cu contents, and hence the OTC of the OCs decreases. The modification of support with a suitable promoter showed the absence of spinel compound by avoiding interaction between active metal and support.[35,36] However, the OTC of these OCs decreased as the number of redox cycles were increased.

The reactivity and durability of CuPA mixed oxides as an OC in the CLC process were examined in this work. Praseodymium metal oxide promoter was chosen because it has good phase stability at a temperature of 1050 °C.[37] In addition, it has good redox properties when exposed to CH_4 and air using Thermogravimetric analysis (TGA).[26] Several preparation methods have been proposed for the synthesis of Cu-based OCs.[35,38] However, the wet impregnation method was considered a more efficient method for Cu-based OCs.[39] Furthermore, the relationship between CuO and Pr-modified γ-Al_2O_3 and the significance of these interactions in the CLC process have never been studied before, emphasizing the uniqueness of the present study. However, this data gap opens the door to misinterpretation and inconsistencies in experimental measurements, especially those collected by the wide-ranging CLC process. Therefore, the present study was focused on examining the performance of the newly developed mixed Cu−Pr/γ-Al_2O_3 oxide in terms of agglomeration, structure stability, and OTC during 10 redox cycles using air and CH_4 gases.

2. METHODOLOGY

2.1. Materials and Reagents. The nitrate precursors of copper (Cu) and praseodymium (Pr) were used to prepare OCs. In addition, for each type of OC, γ alumina (γ-Al_2O_3) was used as a support material. The details of all of the materials used for the synthesis of OCs are given in Table 1.

2.2. Preparation of OCs. Two types of OCs such as 10 wt % Cu/γ-Al_2O_3 (10CuA) and 10 wt % Cu−5 wt % Pr/γ-Al_2O_3 (10CuPA) were prepared using the wet impregnation method.[26] The elemental compositions of 10CuA and 10CuPA for fresh and after 10 cycles in the CLC process are given in Table 2. For 10 g of 10CuA OC, the first 10 wt % of Cu-nitrate was added in deionized (DI) water for the preparation of the Cu-nitrate precursor solution. This Cu-nitrate precursor solution was added drop by drop on γ-Al_2O_3 under continuous mixing for 3 h at room temperature. This mixture was then dried in an oven at 100 °C, and the resulting solid was pulverized in a porcelain mortar. The powder was placed in a ceramic crucible and calcined in a muffle furnace at 450 °C for 4 h. For 10 g of 10CuPA OC, the support (γ-Al_2O_3) was modified first with 5 wt % Pr. The Pr-nitrate precursor solution was prepared in DI water and mixed drop by drop with γ-Al_2O_3 for 3 h at room temperature to achieve 5 wt % Pr loading and dried in an oven at 100 °C. Next, the obtained solid was ground in a porcelain mortar and calcined in a muffle furnace at 450 °C for 4 h. Finally, the as-prepared 5 wt % Pr/γ-Al_2O_3 mixed oxide was mixed with 10 wt % Cu-nitrate precursor solutions for the synthesis of 10CuPA-based OC. The previous steps were repeated for drying, pulverizing, and calcining to get 10 wt % Cu−5 wt % Pr/γ-Al_2O_3 (10CuPA). Figure 1 shows the schematic diagram for the synthesis of OCs.

Table 1. Specifications and Details of the Materials Used for the Preparation of Oxygen Carriers

material name	purity	CAS No	company
γ alumina γ-Al_2O_3	98%	1344-28-1	Merck
copper(II) nitrate trihydrate ($Cu(NO_3)_2{\cdot}3H_2O$)	≥99.5%	10031-43-3	Merck
praseodymium(III) nitrate hexahydrate ($Pr(NO_3)_3{\cdot}6H_2O$)	99.9%	15878-77-0	Sigma-Aldrich

Table 2. Elemental Compositions of 10CuA and 10CuPA Oxygen Carriers

	Cu contents (wt %)		Pr contents (wt %)		γAl_2O_3 (wt %)	
oxygen carriers	theoretical	actual	theoretical	actual	theoretical	actual
10CuA (fresh)	10	7.5			90	92.5
10CuA (after 10 cycles)	10	21.3			90	78.6
10CuPA (fresh)	10	7.9	5	4.3	85	87.7
10CuPA (after 10 cycles)	10	16.4	5	6.7	85	76.7

2.3. Characterizations of OCs. Due to the importance of the chemical, physical, and morphological properties of OCs, the characterization of the synthesized OCs is required for the best efficiency in the CLC process. Furthermore, the bulk and surface properties of OCs have a significant effect on the OTC of OCs during multiple redox properties. Therefore, the information from different characterizations will help improve the performance of OCs in the CLC process. In the present study, the synthesized OCs were characterized using field emission scanning electron microscopy (FESEM), specific surface area analysis, X-ray diffraction (XRD), and temperature-programmed reduction (TPR) analysis. The description of the equipment name and model used for the characterization is given in Table 3.

2.3.1. Surface Morphology. The surface morphologies of all of the fresh (calcined) and used (after 10 redox cycles) OCs were analyzed by field emission scanning electron microscopy (FESEM) analysis using Zeiss Supra 55 VP model. In addition, energy-dispersive X-ray spectroscopy (EDX) was used to study the elemental composition of OCs. Finally, the OC particles

https://doi.org/10.1021/acsomega.2c02993
ACS Omega 2022, 7, 40789−40798

Figure 1. Schematic flowchart for the synthesis of 10CuA- and 10CuPA-based OCs.

Table 3. Details of Equipment Used during Characterization

equipment	model
field emission scanning electron microscope (FESEM)	Zeiss Supra 55 VP
X-ray diffractometer (XRD)	Bruker D8 Advanced Diffractometer
temperature-programmed reduction (TPR) device	TPDRO100

were applied to the copper stub using a 2 min gold layer coating.

2.3.2. X-ray Diffraction. The crystalline phases of the synthesized OCs were analyzed using XRD (Bruker D8 Advance) under the range of 40 kV voltage and 40 mA current using Cu Kα radiations. The samples were scanned at 2θ angles from 10 to 100° with a step size of 2°/min. The identification of the observed diffraction pattern was performed using the MAUD software.

2.3.3. Temperature-Programmed Reduction. The TPR study was performed by the TPDRO100, which was coupled with a thermal conductivity detector (TCD). Approximately, 0.10 g of material was placed into a reactor within the furnace and treated with N_2 gas for 60 min at 200 °C. Then, the gas was changed to 5% H_2/N_2 at a 30 mL/min rate and pretreated at 200 °C for 1 h.

2.4. CLC Experiments. Thermogravimetric analysis (TGA-TA model Q50) was conducted to evaluate the performance of as-prepared OCs. For each type of OC, 15 mg of sample was placed in the platinum pan. The platinum pan was hung in the furnace of TGA by the hang-down wire. The furnace of TGA was closed, and the furnace was heated with a heating rate of 50 °C/min up to 800 °C. The heating of the sample was done in the presence of N_2 gas flowing at a rate of 20 mL/min. For reduction and oxidation processes, 5% CH_4/N_2 (for 3 min) and air (for 10 min) were used at a flow rate of 80 mL/min, respectively. However, the temperature of the furnace is kept constant at 800 °C.[14,18] Between methane and air, nitrogen gas was purged for 3 min to avoid mixing between methane and air. The OTC of OCs during 10 redox cycles was calculated using eq 1.

$$\mathrm{OTC} = \frac{m_{ox} - m_{red}}{m_{ox}} \quad (1)$$

where, m_{ox} is the mass of fully oxidized OC and m_{red} is the mass of fully reduced OC. For an appropriate metal-based OC choice, a total of 10 redox cycles were performed. This experiment was repeated three times, and the average value for OTC was calculated. The schematic diagram for the CLC process using TGA is shown in Figure 2.

3. RESULTS AND DISCUSSION

3.1. FESEM Analysis. The surface morphologies of fresh and used OCs based on 10CuA and 10CuPA were examined using FESEM analysis. Figure 3a,b represents the FESEM images of 10CuA-fresh (calcined) and used (in 10 oxidation−reduction cycles) OCs, respectively. For both fresh and used 10CuA-based OCs, irregular shapes of the particles were observed. It can be noticed that the particle size of 10CuA increased after usage in 10 redox cycles, as shown in Figure 3b. The FESEM images of 10CuPA-fresh (calcined) and after 10 cycles are shown in Figure 3c,d. However, after use in CLC redox cycles, the average particle size of 10CuPA-based OCs decreased. Furthermore, an irregular shape of 10CuPA-based OC particles was examined. Overall, no significant difference in the surface morphologies of 10CuA- and 10CuPA-based OCs was observed. Furthermore, some agglomeration was detected in the morphology of both types of OCs. Energy-dispersive X-ray spectroscopy analysis revealed that the Cu contents increased from 7.5 to 21.3 wt % for 10CuA-fresh and 10CuA-used, respectively. It might be due to the accumulation

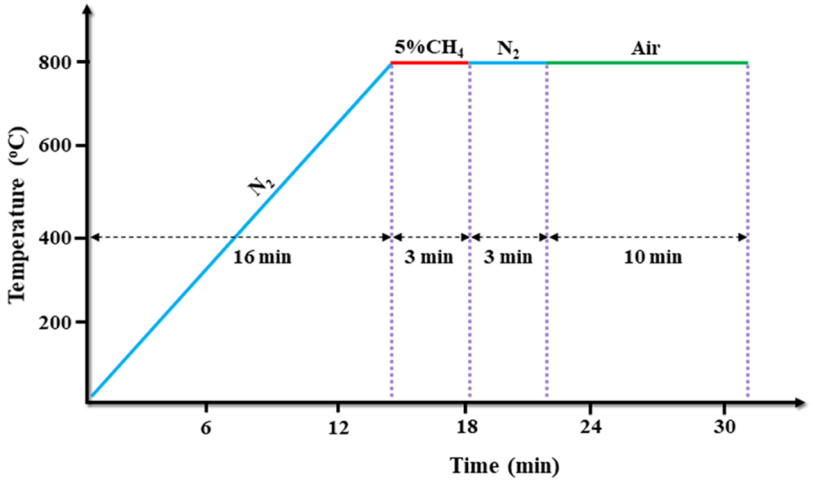

Figure 2. Schematic diagram of the chemical looping combustion process using TGA.

https://doi.org/10.1021/acsomega.2c02993
ACS Omega 2022, 7, 40789−40798

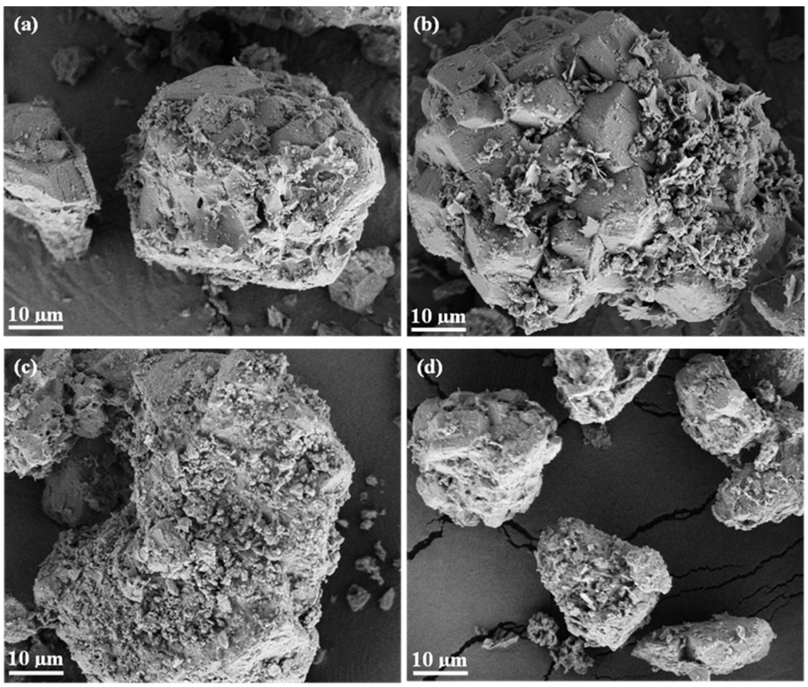

Figure 3. FESEM images of 10CuA-fresh (a) and after 10 cycles (b) and 10CuPA-fresh (c) and after 10 cycles (d).

Table 4. 2θ Angles Corresponding to Different Crystal Phases of 10CuA and 10CuPA Oxygen Carriers

oxygen carrier	crystal phase	2θ angles
10CuA-fresh	CuO	32, 35, 39, 46, 49, 53, 58, 61, 66, 72, and 75°
	$CuAl_2O_4$	NA
	$CuAlO_2$	NA
10CuA-used	CuO	35, 39, 46, and 66°
	$CuAl_2O_4$	31, 37, and 45°
	$CuAlO_2$	31°
10CuPA-fresh	CuO	32, 35, 39, 46, 49, 53, 58, 61, 66, 72, and 75°
	$CuAl_2O_4$	NA
	$CuAlO_2$	NA
10CuPA-used	CuO	32, 35, 39, 46, 49, 53, 58, 61, 66, 72, and 75°
	$CuAl_2O_4$	31, 37, and 45°
	$CuAlO_2$	31°

of copper contents in a specific particle associated with the presence of agglomeration. However, the Cu contents increased from 7.9 to 16.4 wt % for 10CuPA-fresh and 10CuPA-used, respectively. These results showed that the copper contents for 10CuPA-used are more stable than the copper contents for 10CuA-used.

3.2. X-ray Diffraction Analysis. For the crystal structure determination, XRD analysis was executed as shown in Table 4. The XRD findings of 10CuA- and 10CuPA-based OCs are shown in Figure 4. The diffraction peaks associated with CuO at 2θ angles of 32, 35, 39, 46, 49, 53, 58, 61, 66, 72, and 75 were observed.[40] Surprisingly, the peaks corresponding to $CuAl_2O_4$ at 2θ angles of 31, 37, and 45° were also observed.[41] The peak at a 2θ angle of 31° also referred to $CuAlO_2$.[40,41] No peaks were detected for praseodymium oxide because the XRD technique only identifies crystalline phases with a content higher than 5%.[40] For both 10CuA-fresh and 10CuPA-fresh OCs, only peaks corresponding to the CuO crystal phase were observed. However, the peaks related to $CuAl_2O_4$ were not detected. Similar XRD results were reported in the previous studies for Cu-based OCs when a calcination temperature of lower than 600 °C was used.[41] However, the peak intensity of the CuO crystal phase for 10CuA-fresh was higher compared to 10CuPA-fresh. In contrast to this, the peak intensity referred to CuO at 2θ angles of 35°, 39°, 46°, and 66° for 10CuA-used OCs decreased compared to 10CuPA-used OCs. Similarly, the peaks for 10CuA-used associated with the CuO phase at 2θ angles of 32, 49, 53, 58, 61, 72, and 75° completely disappeared in comparison to 10CuPA-used. This might be because the modification of γ-alumina support with praseodymium metal oxide in 10CuPA-used OCs stabilized the CuO contents. For both 10CuA-used and 10CuPA-used OCs, $CuAl_2O_4$ and $CuAlO_2$ crystal phases were detected because the temperature throughout oxidation−reduction cycles was greater than 600 °C. However, the peak intensity corresponding to $CuAl_2O_4$ at a 2θ angle of 37° for 10CuPA-used was lower than 10CuA-used OCs. For both types of OCs, that is, 10CuA-used and 10CuPA-used, the peak related to $CuAlO_2$ was relatively small and existed at the same 2θ angle (31°) for $CuAl_2O_4$. This indicated that the formation of $CuAlO_2$ was relatively low or negligible.

https://doi.org/10.1021/acsomega.2c02993
ACS Omega 2022, 7, 40789−40798

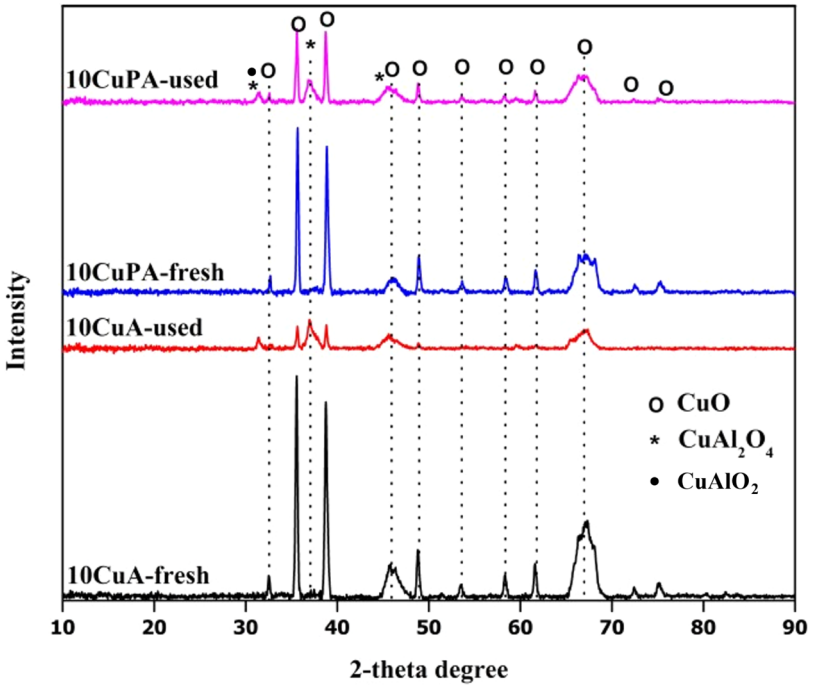

Figure 4. XRD analysis for the 10CuA-fresh (after calcination), 10CuA-used (after 10 redox cycles using 5%CH_4/N_2 and air gases), 10CuPA-fresh, and 10CuPA-used OCs.

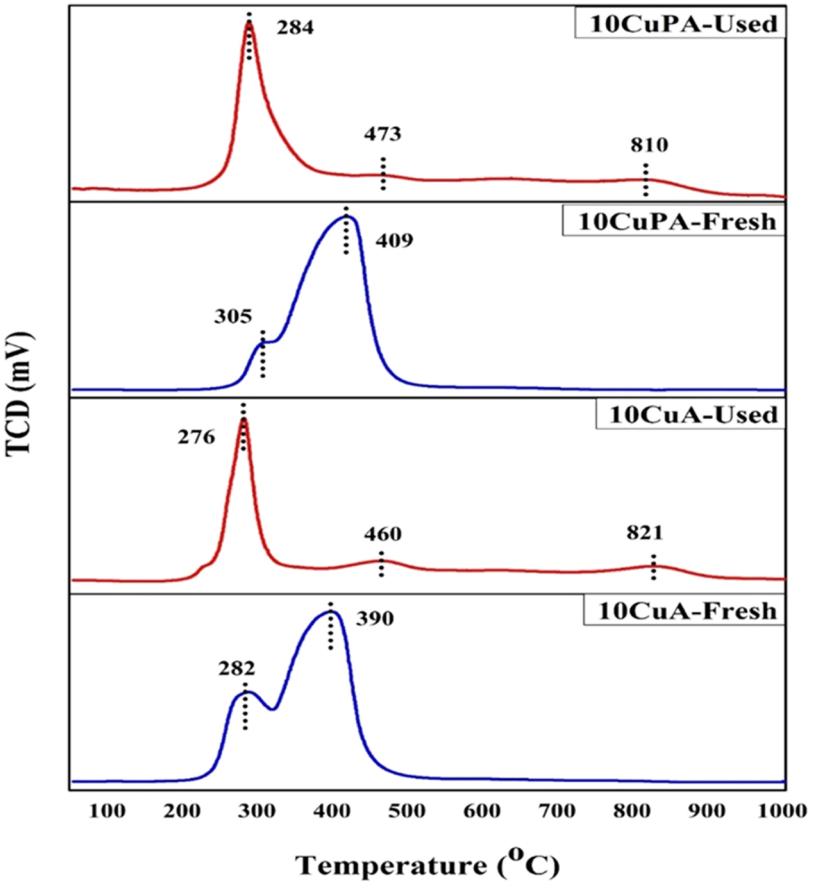

Figure 5. TPR profiles for 10CuA and 10CuPA fresh and used (10 cycles) oxygen carriers.

This strongly suggests that the presence of praseodymium metal oxide reduced the formation of spinel compounds and enhanced the stability of active metal oxide (CuO). A similar effect was noticed in the previous research work; when the contact of active metal with support was minimized, the XRD peaks corresponding to the spinel compound were also

https://doi.org/10.1021/acsomega.2c02993
ACS Omega 2022, 7, 40789−40798

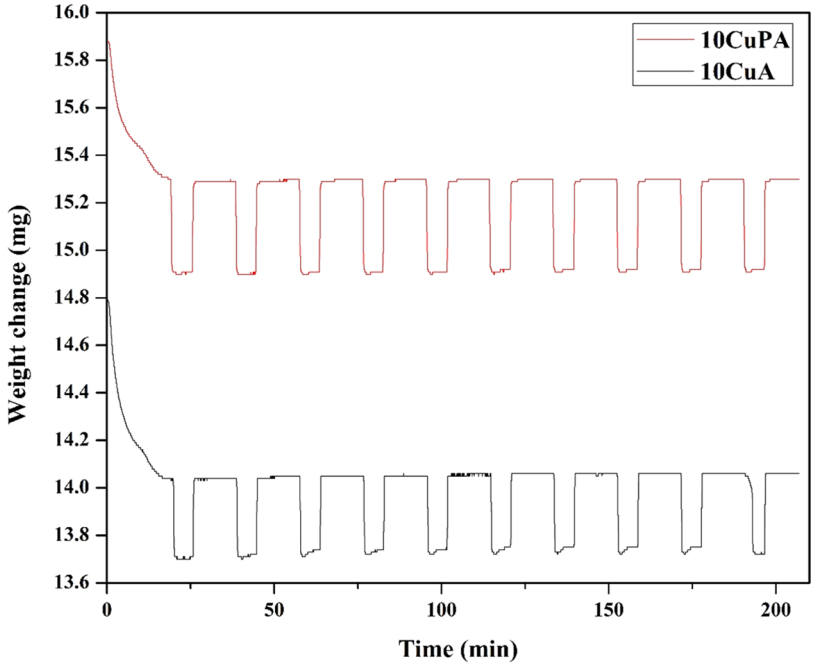

Figure 6. TGA profile for 10CuA- and 10CuPA-based OCs during 10 redox cycles in the CLC process.

decreased.[42] Hence, the addition of praseodymium to a Cu-based OC significantly increased the stability of the OC in terms of uniform distribution of CuO and by lowering the formation of the spinel compound ($CuAl_2O_4$).

3.3. Temperature-Programmed Reduction Analysis. The reduction properties of 10CuA and 10CuPA OCs were investigated using TPR analysis, as shown in Figure 5. The TPR profiles could be decomposed into four different curves at α =270−300 °C, β = 390−410 °C, γ = 450−460 °C, and δ = 800−830 °C. Usually, it is known that the peaks at α and β are attributed to the reduction of well-dispersed CuO and bulk CuO, which are reduced through CuO → Cu, respectively.[40,41] However, the peaks in the range γ contributed to $CuAl_2O_4$ due to strong attraction between CuO and alumina, such as CuO + Al_2O_3 → $CuAl_2O_4$, and peaks at δ associated with reducing $CuAlO_2$.[40] At high temperatures, heating of $CuAl_2O_4$ results in the formation of $CuAlO_2$.[43] The reduction reaction for the spinel compound is prolonged as compared to the CuO. Two possible redox reactions could result in the formation of $CuAlO_2$ at a temperature near 900 °C. The first one is $4CuAl_2O_{4(s)} \rightarrow 4CuAlO_{2(s)} + 2Al_2O_{3(s)} + O_{2(g)}$ and second due to the presence of excess contents of CuO, that is, $2CuAl_2O_{4(s)} + 2CuO_{(s)} \rightarrow 4CuAlO_{2(s)} + O_{2(g)}$.[44]

Figure 5 shows that only two peaks corresponding to α and β appeared for both 10CuA-fresh and 10CuPA-fresh OCs. However, no peaks relevant to $CuAl_2O_4$ and $CuAlO_2$ were found for both 10CuA-fresh and 10CuPA-fresh, owing to the absence of any spinel formation. Similar to XRD results, it is evident that $CuAl_2O_4$ and $CuAlO_2$ were not formed after calcination, possibly due to the low calcination temperature. The peak intensities corresponding to γ and δ for 10CuPA-used OCs were lower than those for 10CuA-used OCs. It shows that higher consumption of H_2 in 10CuA-used OCs is due to the significant formation of spinel compound compared to Pr-promoted, Cu-based OCs. From XRD analysis, similar results were found, which confirmed that the addition of praseodymium lessened the formation of spinel compounds.

3.4. Reactivity with Methane Fuel in Multiple Redox Cycles. Figure 6 shows the weight changes in the carrier as the result of multiple consecutive oxidation/reduction cycles using 5% methane gas for 10CuA and 10CuPA. The OTC of 0.024 (mg of O_2/mg of OC) was achieved for 10CuA-based OCs after 10 redox cycles. In contrast, the OTC of 0.026 (mg of O_2/mg of OC) was attained for 10CuPA-based OCs during 10 cycles. It was examined that owing to the addition of praseodymium oxide in 10CuA-based OCs, the OTC increased by 0.2 wt %. The OTC of 0.026 mg of O_2/mg of OC of 10CuPA in this study remarkably improved compared with the OTC of 10 wt %Cu-γ-Al_2O_3.[40,45,46] Furthermore, the reactivity of 10CuPA in oxidation and reduction reactions was uniform and smooth compared to 10CuA. The standard deviations were found at 0.005 and 0.0002 for 10CuA and 10CuPA, respectively, which provided evidence of good agreement for experimental results. Table 5 presents the confirmation tests for 10CuA- and 10CuPA-based OCs during 10 oxidation−reduction cycles in the CLC process.

The curves of mass-based conversion derived from TGA data for the 10CuA-based OC are shown in Figure 7. The conversion during the reduction phase was around 2.42 wt %

Table 5. Confirmation Results for Oxygen Transport Capacity of Oxygen Carriers at 800 °C Redox Temperature, 3 min Reduction Time and 10 min Oxidation Time in the CLC Process

oxygen carrier	confirmation runs	OTC (mg of O_2/mg of OC)
10CuA OC	run 1	0.0238
	run 2	0.0235
	run 3	0.0245
	standard deviation	0.0005
10CuPA OC	run 1	0.0265
	run 2	0.0260
	run 3	0.0261
	standard deviation	0.0002

https://doi.org/10.1021/acsomega.2c02993
ACS Omega 2022, 7, 40789−40798

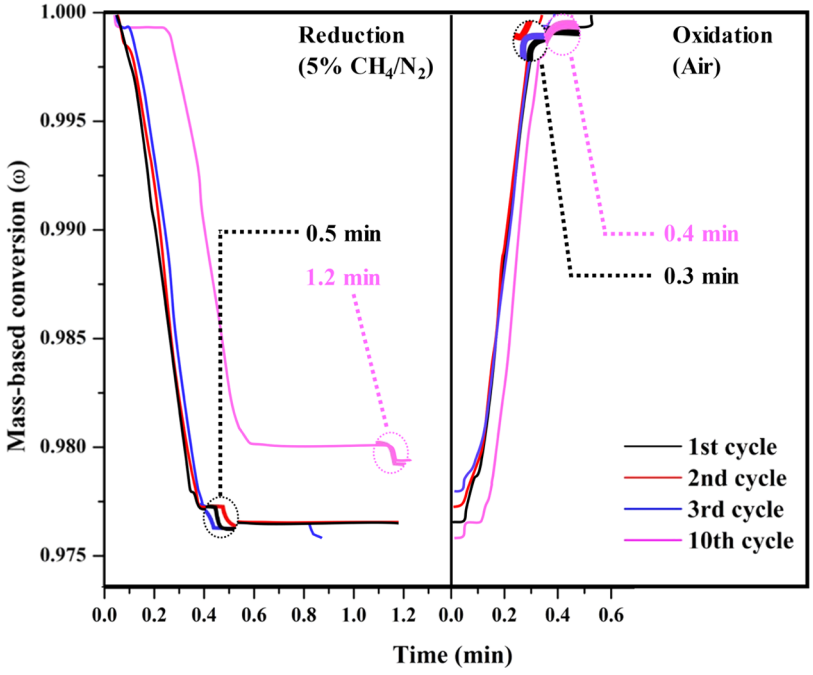

Figure 7. Mass-based conversion profiles for 10CuA-based OC using 5% CH_4/N_2 (reducing gas) and air (oxidizing gas).

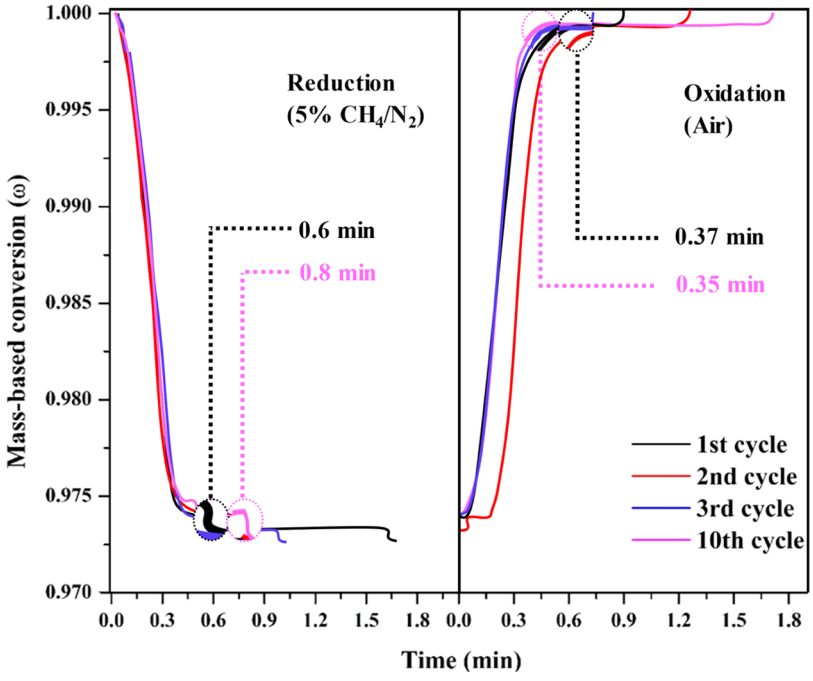

Figure 8. Mass-based conversion profiles for 10CuPA-based OC using 5% CH_4/N_2 (reducing gas) and air (oxidizing gas).

during the first cycle, and it required approximately 0.5 min to complete the reduction process. Thus, the conversion was diminished to 2.41 wt % from the second cycle despite the number of cycles, and the time to complete the reduction was more significant than in the first cycle. As the number of cycles progressed, a longer time was required for the complete reduction. For the 10th cycle, the complete reduction was done in about 1.2 min, which was two times greater than the time for complete reduction in the first cycle. These results suggested that the conversion rate of the 10CuA-based OCs decreased when the number of cycles increased.[47] When OC was exposed to air, the 10CuA-based OC was oxidized. The time required for the first three cycles to complete oxidation was 0.3 min, and a similar mass conversion trend was observed for the first three cycles. However, when the oxidation cycles were increased, it was observed that the time taken by the 10CuA-based OC also increased. The time required for the complete oxidation of the 10th cycle was 0.4 min, which indicated a slower reaction of the reduced OC with oxygen when compared with the first three cycles.

The mass-based conversion profiles of 10CuPA-based OC are shown in Figure 8. The conversion during the reduction phase was around 2.67 wt % in the first cycle, and it required 0.6 min to achieve the entire reduction process. The reduction

https://doi.org/10.1021/acsomega.2c02993
ACS Omega 2022, 7, 40789−40798

period for the 10th cycle was identical to the first cycle (2.67 wt %); however, it lasted nearly 0.8 min to accomplish complete reduction. On the other hand, the time needed for the first cycle to complete the oxidation process was about 0.37 min. The oxidation reaction for 10CuPA-based OC in the second cycle was slower than that in the first cycle, and it took 0.5 min for the entire oxidation process. After the second cycle, the time desired in the following cycles was about 0.35 min for complete oxidation. It was examined that the time required to completely oxidize the 10CuPA-based OC during the 10th cycle was less than in the first cycle. These results revealed that the 10CuPA-based OC shows faster mass-based conversion than 10CuA-based conversion even after 10 oxidation−reduction cycles. This might be because the addition of praseodymium oxide helped to improve the reactivity of the copper-based OC.

In Table 6, the contribution of study has been highlighted by contrasting the OTC of the OC synthesized in the current study with the OC developed in the literature.

Table 6. Oxygen Transport Capacity of the Past Studies Compared with the Present Study of Oxygen Carrier for CLC

type of oxygen carrier	copper loading (wt %)	promoter (wt %)	support	oxygen transport capacity (wt %)	reference
Cu−MgAl	12	27	$MgAl_2O_4$	2.41	40
Cu−NiAl	12.8	3	Al_2O_3	2.57	40
Cu10Al	10		Al_2O_3	2	46
Fe45Al	45		Al2O3	1.3	46
10CuPA	7.9	4.3	Al_2O_3	2.6	present study

4. CONCLUSIONS

This research work was applied to develop chemically and thermally stable OCs for the CLC process. A thermogravimetric analysis was used to investigate the performance of the synthesized OCs for reactivity tests utilizing 5% CH_4/N_2 and air as reducing gas and oxidizing gas, respectively. This work aimed to analyze whether a 10CuPA-based OC could be used as an OC in the CLC process. The oxygen transport capacity (OTC) of a 10CuPA-based OC was 0.0267 mg of O_2/mg of OC, which was higher than the previously reported results without Pr-modified, Cu-based OCs (10CuA). Furthermore, it exhibited high stability in terms of maintaining high OTC as the redox cycles progressed. Both TPR and XRD results revealed that the addition of Pr to Cu-based OCs displayed phase stability even after 10 redox cycles compared to OC without Pr. The FESEM analysis showed that the surface morphology of the 10CuPA-based OC was irregular, and some agglomeration was observed. Although agglomeration was confirmed, it had no impact on the OTC of OC. Hence, these results indicated that the 10CuPA-based OC could become a promising material for use as an OC in the CLC process.

AUTHOR INFORMATION

Corresponding Author

Muhammad Ayoub − *HiCoE, Centre for Biofuel and Biochemical Research (CBBR), Institute of Self-Sustainable Building (ISB), Universiti Teknologi PETRONAS, 32610 Bandar Seri Iskandar, Perak, Malaysia; Department of Chemical Engineering, Universiti Teknologi PETRONAS, 32610 Bandar Seri Iskandar, Perak, Malaysia;* orcid.org/0000-0003-1399-8423; Email: muhammad.ayoub@utp.edu.my

Authors

Muhammad Qasim − *HiCoE, Centre for Biofuel and Biochemical Research (CBBR), Institute of Self-Sustainable Building (ISB), Universiti Teknologi PETRONAS, 32610 Bandar Seri Iskandar, Perak, Malaysia; Department of Chemical Engineering, Universiti Teknologi PETRONAS, 32610 Bandar Seri Iskandar, Perak, Malaysia*

Aqsha Aqsha − *Research Centre on New and Renewable Energy, Institut Teknologi Bandung, 40132 Bandung, Indonesia; Department of Bioenergy Engineering and Chemurgy, Faculty of Industrial Technology, Institut Teknologi Bandung, 45363 Sumedang, Indonesia; Department of Chemical Engineering, Faculty of Industrial Teknology, Institut Teknologi Bandung, 40132 Bandung, Indonesia;* orcid.org/0000-0002-9345-0910

Nur Adibah Ghazali − *HiCoE, Centre for Biofuel and Biochemical Research (CBBR), Institute of Self-Sustainable Building (ISB), Universiti Teknologi PETRONAS, 32610 Bandar Seri Iskandar, Perak, Malaysia; Department of Chemical Engineering, Universiti Teknologi PETRONAS, 32610 Bandar Seri Iskandar, Perak, Malaysia*

Sami Ullah − *Department of Chemistry, College of Science, King Khalid University, 61413 Abha, Saudi Arabia;* orcid.org/0000-0002-9669-5737

Yoshito Ando − *Collaborative Research Centre for Green Materials on Environmental Technology, Kyushu Institute of Technology, 808-0196 Fukuoka, Japan;* orcid.org/0000-0003-3839-0705

Sarah Farrukh − *Department of Chemical Engineering, School of Chemical and Materials Engineering, National University of Sciences and Technology, H-12 Islamabad, Pakistan*

Complete contact information is available at: https://pubs.acs.org/10.1021/acsomega.2c02993

Notes

The authors declare no competing financial interest.

ACKNOWLEDGMENTS

The authors are grateful to HiCOE, the Centre for Biofuel and Biochemical Research (CBBR), for their support. This research was funded by the International Collaborative Research Fund (015ME0-271), Yayasan Universiti Teknologi PETRONAS (YUTP, 015LC0-331), and the Ministry of Education (MOE) through the Fundamental Research Grant Scheme, FRGS/1/2018/TK02/UTP/03/2.

REFERENCES

(1) Wang, X.; Chen, Z.; Hu, M.; Tian, Y.; Jin, X.; Ma, S.; Xu, T.; Hu, Z.; Liu, S.; Guo, D.; Xiao, B. Chemical looping combustion of biomass using metal ferrites as oxygen carriers. *Chem. Eng. J.* **2017**, *312*, 252−262.

(2) Rubin, E. S.; Chen, C.; Rao, A. B. Cost and performance of fossil fuel power plants with CO2 capture and storage. *Energy Policy* **2007**, *35*, 4444−4454.

(3) Zhao, Y.-j.; Zhang, Y.-k.; Cui, Y.; Duan, Y.-y.; Huang, Y.; Wei, G.-q.; Mohamed, U.; Shi, L.-j.; Yi, Q.; Nimmo, W. Pinch combined with exergy analysis for heat exchange network and techno-economic evaluation of coal chemical looping combustion power plant with CO2 capture. *Energy* **2022**, *238*, No. 121720.

https://doi.org/10.1021/acsomega.2c02993
ACS Omega 2022, 7, 40789−40798

(4) Hossain, M. M.; de Lasa, H. I. Chemical-looping combustion (CLC) for inherent CO2 separations—a review. *Chem. Eng. Sci.* **2008**, *63*, 4433−4451.
(5) Zhu, L.; He, Y.; Li, L.; Wu, P. Tech-economic assessment of second-generation CCS: Chemical looping combustion. *Energy* **2018**, *144*, 915−927.
(6) Velasco-Sarria, F. J.; Forero, C. R.; Adánez-Rubio, I.; Abad, A.; Adánez, J. Assessment of low-cost oxygen carrier in South-western Colombia, and its use in the in-situ gasification chemical looping combustion technology. *Fuel* **2018**, *218*, 417−424.
(7) Di, Z.; Cao, Y.; Yang, F.; Cheng, F.; Zhang, K. Studies on steel slag as an oxygen carrier for chemical looping combustion. *Fuel* **2018**, *226*, 618−626.
(8) Mayer, K.; Penthor, S.; Pröll, T.; Hofbauer, H. The different demands of oxygen carriers on the reactor system of a CLC plant—Results of oxygen carrier testing in a 120kWth pilot plant. *Appl. Energy* **2015**, *157*, 323−329.
(9) Tijani, M. M.; Aqsha, A.; Mahinpey, N. Synthesis and study of metal-based oxygen carriers (Cu, Co, Fe, Ni) and their interaction with supported metal oxides (Al2O3, CeO2, TiO2, ZrO2) in a chemical looping combustion system. *Energy* **2017**, *138*, 873−882.
(10) Imtiaz, Q.; Armutlulu, A.; Donat, F.; Naeem, M. A.; Müller, C. R. Preventing Agglomeration of CuO-Based Oxygen Carriers for Chemical Looping Applications. *ACS Sustainable Chem. Eng.* **2021**, *9*, 5972−5980.
(11) Durmaz, M.; Dilmaç, N.; Dilmaç, Ö. F. Evaluation of performance of copper converter slag as oxygen carrier in chemical-looping combustion (CLC). *Energy* **2020**, *196*, No. 117055.
(12) Miller, D. D.; Smith, M.; Shekhawat, D. Development of Fe-based oxygen carrier using spent FCC catalyst as support for high temperature chemical looping combustion. *Fuel* **2020**, *259*, No. 116239.
(13) Ma, Z.; Liu, G.; Lu, Y.; Wang, J.; Zhang, H. Improved redox performance of Fe2O3/Al2O3 oxygen carrier via element doping in chemical looping combustion. *Fuel Process. Technol.* **2021**, *224*, No. 107030.
(14) Ghazali, N. A.; Aqsha, A.; Komiyama, M.; Qasim, M.; Mohd Yusoff, M. H.; Ayoub, M.; Ameen, M.; Tijani, M. M. Comparative Study on Ni/γ-Al2O3 Prepared via Ultrasonic Irradiation and Impregnation Approaches as an Oxygen Carrier in Chemical Looping Combustion. *Ind. Eng. Chem. Res.* **2021**, *60*, No. 13542.
(15) Lin, S.; Gu, Z.; Zhu, X.; Wei, Y.; Long, Y.; Yang, K.; He, F.; Wang, H.; Li, K. Synergy of red mud oxygen carrier with MgO and NiO for enhanced chemical-looping combustion. *Energy* **2020**, *197*, No. 117202.
(16) Li, Y.; Li, Z.; Liu, L.; Cai, N. Measuring the fast oxidation kinetics of a manganese oxygen carrier using microfluidized bed thermogravimetric analysis. *Chem. Eng. J.* **2020**, *385*, No. 123970.
(17) Güleç, F.; Meredith, W.; Sun, C.-G.; Snape, C. E. Selective low temperature chemical looping combustion of higher alkanes with Cu- and Mn- oxides. *Energy* **2019**, *173*, 658−666.
(18) Son, E. N.; Baek, S. H.; Lee, R.; Baek, J. I.; Ryu, H. J.; Yoo, D. J.; Sohn, J. M. Study on the redox characteristics of CaCo based oxygen carrier for Chemical Looping Combustion. *Chem. Eng. J.* **2019**, *377*, No. 121522.
(19) Linderholm, C.; Abad, A.; Mattisson, T.; Lyngfelt, A. 160 h of chemical-looping combustion in a 10 kW reactor system with a NiO-based oxygen carrier. *Int. J. Greenhouse Gas Control* **2008**, *2*, 520−530.
(20) Kolbitsch, P.; Bolhar-Nordenkampf, J.; Pröll, T.; Hofbauer, H. Comparison of two Ni-based oxygen carriers for chemical looping combustion of natural gas in 140 kW continuous looping operation. *Ind. Eng. Chem. Res.* **2009**, *48*, 5542−5547.
(21) Adánez, J.; Gayán, P.; Celaya, J.; de Diego, L. F.; García-Labiano, F.; Abad, A. Chemical Looping Combustion in a 10 kWth Prototype Using a CuO/Al2O3 Oxygen Carrier: Effect of Operating Conditions on Methane Combustion. *Ind. Eng. Chem. Res.* **2006**, *45*, 6075−6080.
(22) Ryu, H.-J.; Jin, G.-T.; Yi, C.-K.Demonstration of Inherent CO2 Separation and no NOx Emission in a 50kW Chemical-Looping Combustor: Continuous Reduction and Oxidation Experiment. In *International Journal of Greenhouse Gas Control 7*, Rubin, E. S.; Keith, D. W.; Gilboy, C. F.; Wilson, M.; Morris, T.; Gale, J.; Thambimuthu, K. Eds.; Elsevier Science Ltd, 2005; pp 1907−1910.
(23) Cho, P.; Mattisson, T.; Lyngfelt, A. Carbon Formation on Nickel and Iron Oxide-Containing Oxygen Carriers for Chemical-Looping Combustion. *Ind. Eng. Chem. Res.* **2005**, *44*, 668−676.
(24) Adánez, J.; de Diego, L. F.; García-Labiano, F.; Gayán, P.; Abad, A.; Palacios, J. M. Selection of Oxygen Carriers for Chemical-Looping Combustion. *Energy Fuels* **2004**, *18*, 371−377.
(25) Izquierdo, M. T.; García-Labiano, F.; Abad, A.; Cabello, A.; Gayán, P.; de Diego, L. F.; Adánez, J. On the optimization of physical and chemical stability of a Cu/Al2O3 impregnated oxygen carrier for chemical looping combustion. *Fuel Process. Technol.* **2021**, *215*, No. 106740.
(26) Qasim, M.; Ayoub, M.; Aqsha, A.; Ghazali, N. A. Investigation and Comparison for the Redox Behavior of Different Metal Oxides (Ni, Fe, Co, Cu, Ce, La, Pr) with and without Gamma-Alumina Support for the Chemical Looping Combustion. *Solid State Technol.* **2020**, *63*, 19450−19460.
(27) Tian, X.; Su, M.; Zhao, H. Kinetics of redox reactions of CuO@TiO2−Al2O3 for chemical looping combustion and chemical looping with oxygen uncoupling. *Combust. Flame* **2020**, *213*, 255−267.
(28) Bhavsar, S.; Isenberg, N.; More, A.; Veser, G. Lanthana-doped ceria as active support for oxygen carriers in chemical looping combustion. *Appl. Energy* **2016**, *168*, 236−247.
(29) Adánez-Rubio, I.; Bararpour, S. T.; Abad, A.; Gayán, P.; Williams, G.; Scullard, A.; Mahinpey, N.; Adánez, J. Performance Evaluation of a Cu-Based Oxygen Carrier Impregnated onto ZrO2 for Chemical-Looping Combustion (CLC). *Ind. Eng. Chem. Res.* **2020**, *59*, 7255−7266.
(30) Cabello, A.; Gayán, P.; García-Labiano, F.; de Diego, L. F.; Abad, A.; Adánez, J. On the attrition evaluation of oxygen carriers in Chemical Looping Combustion. *Fuel Process. Technol.* **2016**, *148*, 188−197.
(31) Qasim, M.; Ayoub, M.; Ghazali, N. A.; Aqsha, A.; Ameen, M. Recent advances and development of various oxygen carriers for the chemical looping combustion process: a review. *Ind. Eng. Chem. Res.* **2021**, *60* (24), 8621−8641.
(32) Imtiaz, Q.; Kurlov, A.; Rupp, J. L. M.; Müller, C. R. Highly Efficient Oxygen-Storage Material with Intrinsic Coke Resistance for Chemical Looping Combustion-Based CO2 Capture. *ChemSusChem* **2015**, *8*, 2055−2065.
(33) Dai, J.; Hughey, L.; Whitty, K. J. Influence of fuel ash on the recoverability of copper from the spent material of chemical looping combustion. *Fuel Process. Technol.* **2020**, *201*, No. 106358.
(34) de Diego, L. F.; Gayán, P.; García-Labiano, F.; Celaya, J.; Abad, A.; Adánez, J. Impregnated CuO/Al2O3 Oxygen Carriers for Chemical-Looping Combustion: Avoiding Fluidized Bed Agglomeration. *Energy Fuels* **2005**, *19*, 1850−1856.
(35) Ma, J.; Mei, D.; Peng, W.; Tian, X.; Ren, D.; Zhao, H. On the high performance of a core-shell structured CaO-CuO/MgO@Al2O3 material in calcium looping integrated with chemical looping combustion (CaL-CLC). *Chem. Eng. J.* **2019**, *368*, 504−512.
(36) Qasim, M.; Ayoub, M.; Aqsha, A.; Zulfiqar, M. Preparation of Metal Oxide-based Oxygen Carriers Supported with CeO2 and γ-Al2O3 for Chemical Looping Combustion. *Chem. Eng. Technol.* **2021**, *44*, 782−787.
(37) Zhou, G.; Gorte, R. J. Thermodynamic Investigation of the Redox Properties for Ceria−Hafnia, Ceria−Terbia, and Ceria−Praseodymia Solid Solutions. *J. Phys. Chem. B* **2008**, *112*, 9869−9875.
(38) Kuang, C.; Wang, S.; Luo, M.; Zhao, J. Reactivity study and kinetic evaluation of CuO-based oxygen carriers modified by three different ores in Chemical looping with oxygen uncoupling (CLOU) process. *Chin. J. Chem. Eng.* **2021**, *37*, 54−63.
(39) De Diego, L. F.; García-Labiano, F.; Adánez, J.; Gayán, P.; Abad, A.; Corbella, B. M.; Palacios, J. M. Development of Cu-based oxygen carriers for chemical-looping combustion. *Fuel* **2004**, *83*, 1749−1757.

https://doi.org/10.1021/acsomega.2c02993
ACS Omega 2022, 7, 40789−40798

(40) Gayán, P.; Forero, C. R.; Abad, A.; de Diego, L. F.; García-Labiano, F.; Adánez, J. Effect of Support on the Behavior of Cu-Based Oxygen Carriers during Long-Term CLC Operation at Temperatures above 1073 K. *Energy Fuels* **2011**, *25*, 1316−1326.
(41) Luo, M.-F.; Fang, P.; He, M.; Xie, Y.-L. In situ XRD, Raman, and TPR studies of CuO/Al2O3 catalysts for CO oxidation. *J. Mol. Catal. A: Chem.* **2005**, *239*, 243−248.
(42) Ahmed, I.; de Lasa, H. Syngas chemical looping combustion using a highly performing fluidizable oxygen carrier. *Catal. Today* **2020**, *343*, 63−71.
(43) Artizzu, P.; Garbowski, E.; Primet, M.; Brulle, Y.; Saint-Just, J. Catalytic combustion of methane on aluminate-supported copper oxide. *Catal. Today* **1999**, *47*, 83−93.
(44) Hu, W.; Donat, F.; Scott, S.; Dennis, J. The interaction between CuO and Al2O3 and the reactivity of copper aluminates below 1000 °C and their implication on the use of the Cu−Al−O system for oxygen storage and production. *RSC Adv.* **2016**, *6*, 113016−113024.
(45) Abad, A.; García-Labiano, F.; de Diego, L. F.; Gayán, P.; Adánez, J. Reduction Kinetics of Cu-, Ni-, and Fe-Based Oxygen Carriers Using Syngas (CO + H2) for Chemical-Looping Combustion. *Energy Fuels* **2007**, *21*, 1843−1853.
(46) García-Labiano, F.; Adánez, J.; de Diego, L. F.; Gayán, P.; Abad, A. Effect of Pressure on the Behavior of Copper-, Iron-, and Nickel-Based Oxygen Carriers for Chemical-Looping Combustion. *Energy Fuels* **2006**, *20*, 26−33.
(47) Donat, F.; Hu, W.; Scott, S. A.; Dennis, J. S. Characteristics of Copper-based Oxygen Carriers Supported on Calcium Aluminates for Chemical-Looping Combustion with Oxygen Uncoupling (CLOU). *Ind. Eng. Chem. Res.* **2015**, *54*, 6713−6723.

https://doi.org/10.1021/acsomega.2c02993
ACS Omega 2022, 7, 40789−40798